

6-16-2017

The spectral and chemical measurement of pollutants on snow near South Pole, Antarctica

Kimberly A. Casey

Susan D. Kaspari

S. M. Skiles

K. Kreutz

M. J. Handley

Follow this and additional works at: <https://digitalcommons.cwu.edu/cotsfac>



Part of the [Climate Commons](#), and the [Environmental Sciences Commons](#)

RESEARCH ARTICLE

10.1002/2016JD026418

Key Points:

- South Pole station fossil fuel combustion has a measurable regional impact in increasing impurity concentrations and reducing snow albedo
- Snow with high trace element and black carbon concentrations was associated with radiative forcing up to 70 W m^{-2}
- Measured snow albedo differed from modeled snow albedo due to specific elemental composition of impurities

Correspondence to:

K. A. Casey,
kimberly.a.casey@nasa.gov

Citation:

Casey, K. A., S. D. Kaspari, S. M. Skiles, K. Kreutz, and M. J. Handley (2017), The spectral and chemical measurement of pollutants on snow near South Pole, Antarctica, *J. Geophys. Res. Atmos.*, 122, 6592–6610, doi:10.1002/2016JD026418.

Received 21 DEC 2016

Accepted 13 MAY 2017

Accepted article online 17 MAY 2017

Published online 16 JUN 2017

The spectral and chemical measurement of pollutants on snow near South Pole, Antarctica

K. A. Casey^{1,2,3} , S. D. Kaspari⁴ , S. M. Skiles⁵, K. Kreutz^{6,7} , and M. J. Handley⁶

¹Earth System Science Interdisciplinary Center, University of Maryland, College Park, Maryland, USA, ²Cryospheric Sciences Laboratory, NASA Goddard Space Flight Center, Greenbelt, Maryland, USA, ³Now at Land Remote Sensing Program, U.S. Geological Survey, Reston, Virginia, USA, ⁴Department of Geological Sciences, Central Washington University, Ellensburg, Washington, USA, ⁵Department of Geography, University of Utah, Salt Lake City, Utah, USA, ⁶School of Earth and Climate Sciences, University of Maine, Orono, Maine, USA, ⁷Climate Change Institute, University of Maine, Orono, Maine, USA

Abstract Remote sensing of light-absorbing particles (LAPs), or dark colored impurities, such as black carbon (BC) and dust on snow, is a key remaining challenge in cryospheric surface characterization and application to snow, ice, and climate models. We present a quantitative data set of in situ snow reflectance, measured and modeled albedo, and BC and trace element concentrations from clean to heavily fossil fuel emission contaminated snow near South Pole, Antarctica. Over 380 snow reflectance spectra (350–2500 nm) and 28 surface snow samples were collected at seven distinct sites in the austral summer season of 2014–2015. Snow samples were analyzed for BC concentration via a single particle soot photometer and for trace element concentration via an inductively coupled plasma mass spectrometer. Snow impurity concentrations ranged from 0.14 to 7000 part per billion (ppb) BC, 9.5 to 1200 ppb sulfur, 0.19 to 660 ppb iron, 0.013 to 1.9 ppb chromium, 0.13 to 120 ppb copper, 0.63 to 6.3 ppb zinc, 0.45 to 82 parts per trillion (ppt) arsenic, 0.0028 to 6.1 ppb cadmium, 0.062 to 22 ppb barium, and 0.0044 to 6.2 ppb lead. Broadband visible to shortwave infrared albedo ranged from 0.85 in pristine snow to 0.62 in contaminated snow. LAP radiative forcing, the enhanced surface absorption due to BC and trace elements, spanned from $<1 \text{ W m}^{-2}$ for clean snow to $\sim 70 \text{ W m}^{-2}$ for snow with high BC and trace element content. Measured snow reflectance differed from modeled snow albedo due to specific impurity-dependent absorption features, which we recommend be further studied and improved in snow albedo models.

1. Introduction

Snow purity and reflectivity affects local, regional, and global radiative energy balance and is a key component in the climate system. Snow in the clean air sector near South Pole, Antarctica, is one of the most clean, reflective surfaces on Earth. Yet areas near the Amundsen-Scott South Pole Station (hereafter South Pole Station) are subject to intense fossil fuel emissions where black carbon (BC), dust, metals, organic matter, and other light-absorbing particles (LAPs) become deposited on and darken snow. Such LAPs deposited and engrained within snow result in reduced surface snow albedo, increased absorption of solar radiation, and in turn accelerated snow metamorphism and melt processes, contributing to a snow albedo feedback mechanism [e.g., Warren and Wiscombe, 1980; Painter et al., 2007; Kaspari et al., 2015]. Quantification of snow composition is crucial to accurately understand radiative energy balance.

Spectroscopy, the study of light reflected, scattered, or emitted as a function of wavelength, is used to quantify snow optical properties. Clean, fine-grained snow is scattering dominated and reflects the majority (97–99%) of incident sunlight in UV to visible wavelengths (350–750 nm) and is more absorbing in near to shortwave infrared wavelengths (NIR/SWIR, 750–2500 nm) [Warren, 1982]. LAPs can darken the snow surface and dominate visible reflective signatures [Warren et al., 1993] with discrete or broad absorption features indicative of component elements and/or molecules [Clark, 1999]. In general, dust yields visible absorption features, while BC reduces snow reflectance in a broader manner from visible toward shortwave infrared [Warren and Wiscombe, 1980]. The dominating factor of snow reflectivity shifts from LAPs in the UV and visible to snow grain size in NIR/SWIR, where longer path lengths through larger snow grains decrease snow reflectivity. The difference in absorbed energy due to LAPs, or radiative forcing, can enhance the rate of snow grain growth, and therefore, LAPs can impact the full range of snow reflectance [Hansen and Nazarenko, 2004; Painter et al., 2012].

In situ snow spectroscopy and coincident collection and analysis of snow samples can be used to quantify physical properties, chemical composition, and radiative impacts of LAPs in snow. These measurements are sparse since fieldwork to collect spectroscopy and physical samples and subsequent chemical analysis is expensive, time consuming, and subject to harsh environmental conditions. Still, there are a number of studies that have directly measured LAPs concentrations in snow and ice, aiming at constraining LAP radiative forcing, namely, BC and dust [Skiles *et al.*, 2012; Kaspari *et al.*, 2014, 2015; Jacobi *et al.*, 2015], distribution of LAPs in melting snow [Doherty *et al.*, 2013; Skiles and Painter, 2016], and composition of particulates on cryospheric surfaces in comparison to spectral reflectance signatures [Casey *et al.*, 2012; Tedesco *et al.*, 2013]. Research continues to progress regarding the optical properties of BC and dust in snow [e.g., Bond and Bergstrom, 2006; Kuchiki *et al.*, 2009; Skiles *et al.*, 2016; Khan *et al.*, 2017]. Laboratory studies have also been conducted. Hadley and Kirchstetter [2012] measured BC albedo reduction (concentrations of 0–1,700 ppb BC) as a function of snow grain size (55, 65, and 110 μm) in laboratory snow and compared to modeled albedo estimates of snow containing BC and found good agreement between the laboratory measured and modeled snow albedos (given solar zenith angle of 0°).

Within the clean air sector grid east-northeast of South Pole Station, the snow and atmosphere are protected from air, vehicle, and recreational traffic (Figure 1). Nominal winds move from 45°E grid southwest and prevent the clean air sector from receiving most South Pole Station and science camp-related pollution. Sporadic storm or weather events can alter nominal wind directions, though winds rarely move grid northeast, thus rarely transport station area pollutants into the clean air sector. Measurement of atmospheric and snow properties in the clean air sector has been conducted for several decades (e.g., NOAA Earth System Research Laboratory, South Pole Observatory), including study of snow albedo [Hoinkes, 1960; Hanson, 1960] and background atmospheric and snow constituent concentrations [Keeling *et al.*, 1976; Kumai, 1976; Hogan *et al.*, 1982; Boutron, 1982; Bodhaine *et al.*, 1986; Bergin *et al.*, 1998]. In the clean air sector, Hansen *et al.* [1988] found atmospheric background concentrations of BC to generally range from 50 pg m^{-3} to 5 ng m^{-3} . Warren *et al.* [2006] found background (clean air sector) dust content in modern snow at South Pole to be 15 ppb and soot to be 0.1–0.3 ppb.

In contrast to the clean air sector, elevated levels of pollutants have been reported in snow near and downwind of South Pole Station operation facilities and science camps [e.g., Warren *et al.*, 2006]. South Pole Station operations and science camps necessitate burning of fossil fuels in generators, vehicles, and aircraft. Aviation grade fuels with ice inhibitors to suppress the freezing point to approximately -100°C are the primary fuels used in aircraft and large generators at South Pole Station [Brier *et al.*, 1998]. From a South Pole Station Environmental Impact Statement released in 1998, personnel and cargo LC-130 aircraft transport represented 75% of South Pole Station operation fossil fuel combustion, with nominally approximately 200 flights per year [Brier *et al.*, 1998]. Since roughly 2006, resupply surface traverses from coastal McMurdo to South Pole Stations now are another main source of food, fuel, and other required materials, reducing annual aircraft transport to South Pole Station. The specific percentage of flight to traverse delivered supplies is customized to support cargo, fuel, and transport needs from year to year [Jung *et al.*, 2004]. Approximately 1% of the fuel used at South Pole Station is unleaded gasoline, used in vehicles and small engines, primarily in austral summers [Brier *et al.*, 1998]. In addition to combustion, fuel volatilization and occasionally spills or leaks occur during handling and transport of fuels to storage vessels depositing pollutants on the snow near South Pole [Brier *et al.*, 1998].

Fuel combustion emissions vary with engine type, load, and specific fuel [Tesseraux, 2004], though are known to include sulfur dioxide [Shirsat and Graf, 2009], nitrogen oxides [Barrie, 1996], carbon monoxide, hydrocarbons [Nazarenko *et al.*, 2016] and particles, including metalloid and metal elements such as Cr, Mn, Fe, Co, Cu, Zn, As, Cd, Ba, and Pb [Miner, 1969; Schroeder, 1970; Ng and Patterson, 1982; Vouk and Piver, 1983; Barrie, 1996]. Petroleum hydrocarbon diesel fuels (jet-propulsion fuel 8, JP-8, AN-8) are the primary fuels used at South Pole Station for aircraft and large generators. These fuels contain proprietary formulations of ice, static, and corrosion inhibitor agents, and exact fuel compositions vary from batch to batch [National Research Council, 2003]. Thus, discernment of emission particles remains challenging [McDougal and Rogers, 2004]. At the South Pole, annual baseline emissions of particles were estimated at 820 kg/yr for aircraft and 1500 kg/yr for power generation, heating and water production, and equipment operations [Brier *et al.*, 1998].

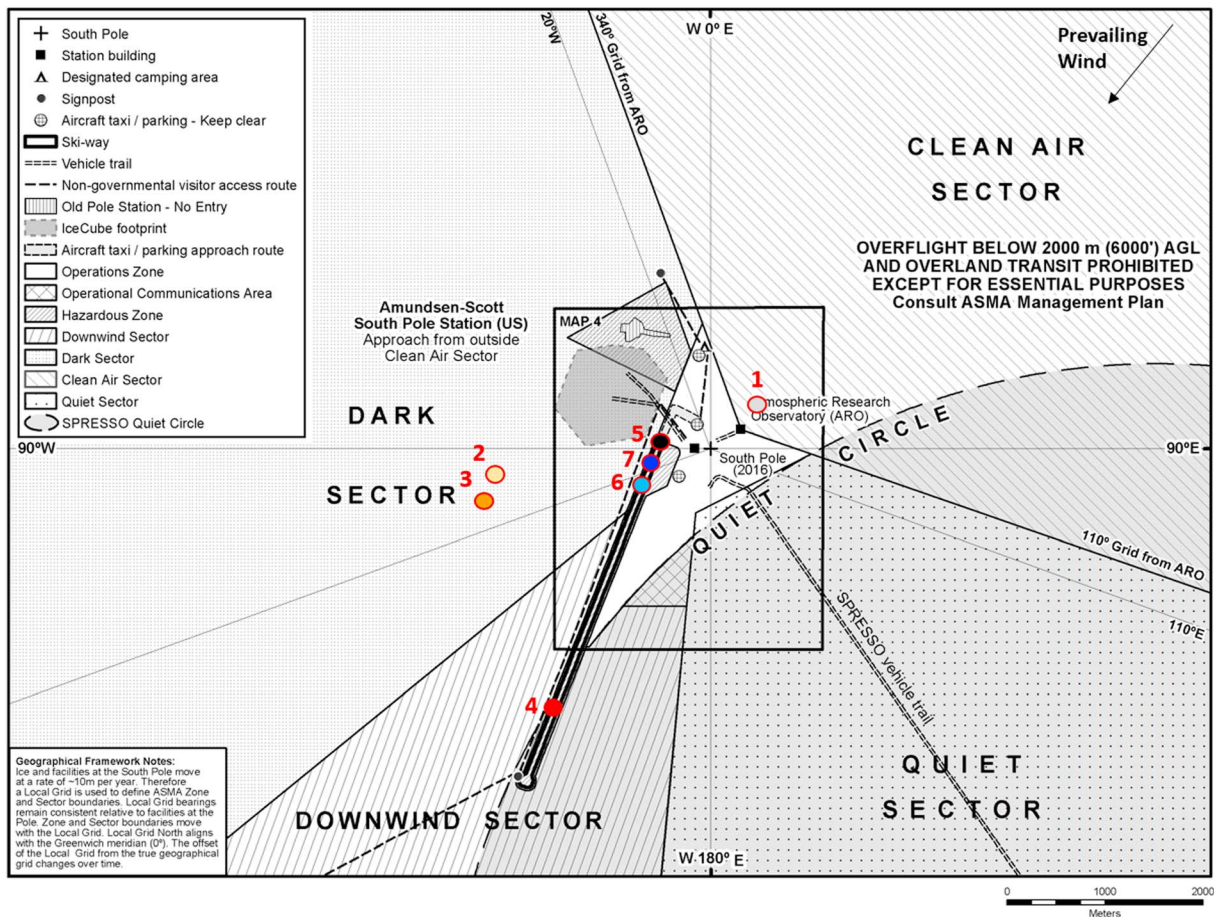


Figure 1. Snow spectral and surface sample sites are identified on the United States Antarctic Program logistic map.

Surface snow particle composition near Antarctic stations has been targeted by several studies. *Boutron and Wolff* [1989] found that emissions from fuel and waste burning at multiple Antarctic station settlements enhance concentrations of S, Pb, Zn, Cd, and Cu in Antarctic snow compared to background atmospheric fall-out. *Suttie and Wolff* [1993] reported Halley research station Antarctic surface snow samples to contain Cu, Cd, Pb, and Zn heavy metal concentrations of up to 800,000 times background levels directly in the path (within 0–20 m) of emission exhaust. *Warren and Clarke* [1990] were among the first to measure atmospheric and snow surface BC concentrations and map emission fallout patterns around South Pole from December 1985 to February 1986, finding that the heaviest particulate deposition occurs within ~1 km of emission sources. The concentrations of some heavy metals have been reported to have increased at South Pole in recent decades due to anthropogenic emissions. For example, Pb was measured at ~4–5 times background levels since 1960s [*Boutron, 1982; McConnell et al., 2014*], and Ba concentration was found to be a factor of ~23 greater since 1980 [*Korotkikh et al., 2014*].

Although relatively low concentrations of LAPs on snow and ice have proven to be difficult to resolve with optical satellite remote sensing data (e.g., Greenland snow BC average annual concentrations of ~3 ppb reported in *Polashenski et al. [2015]*), heavy concentrations of LAPs on snow and ice are easily apparent in optical airborne and satellite remote sensing data (e.g., Advanced Spaceborne Thermal Emission and Reflection Radiometer satellite image 18105261, acquired 10 May 2003, of coal mining in Svalbard, Norway; BC concentrations of 345 ppb refractory BC and 4863 ppb effective BC, reported in *Khan et al. [2017]*; pollution on snow, [*Simões and Zagorodnov, 2001*]; and ablation zone in Greenland, [*Wientjes and Oerlemans, 2010*]). Greater magnitude impurity concentrations on snow and ice can not only be detected with remote sensing but also geochemically differentiated [*Gleeson et al., 2010; Casey and Kääh, 2012*]. The Snow Grain Size and Pollution amount algorithm, used with Moderate Resolution Imaging

Spectroradiometer (MODIS), retrieves soot concentrations with 10% accuracy when BC concentrations are greater than 1000 ppb [Zege *et al.*, 2011]. The daily MODIS dust radiative forcing in snow product is available in near-real time and historically for areas of the globe known for dust on snow deposition (e.g., Western U.S. and Hindu-Kush-Himalaya), but due to the coarse spatial and spectral resolution, retrieved values are subject to relatively high uncertainties [Painter *et al.*, 2012]. Although remote sensing of LAPs in snow and ice remains a complex task (many challenges detailed in Warren [2013]), we hypothesize that high concentrations of LAPs and resulting radiative impacts can continue to be further characterized with remote sensing techniques.

To address the paucity of heavily contaminated snow spectral and chemical data, the South Pole region's gradient of very clean to exceptionally polluted snow over small spatial scales was targeted for study. Here we present a comprehensive data set of snow spectroscopy, black carbon, and trace element concentrations to quantify fossil fuel emissions on snow and consequent radiative impacts. This study improves our general understanding of the impacts of LAPs on snow and can contribute to advancing cryospheric remote sensing techniques. Greater understanding of snow and ice LAPs concentrations and radiative impacts is crucial to quantifying air-to-snow chemical interactions, aerosol climate connections, radiative energy balance, and cryospheric mass balance [Hansen and Nazarenko, 2004; Flanner *et al.*, 2007; Koch *et al.*, 2009; Intergovernmental Panel on Climate Change, 2014; Goelles *et al.*, 2015; Qian *et al.*, 2015].

2. Study Location

Located in central Antarctica, at an elevation of 2835 meters above sea level, the South Pole is climatically influenced by both the conditions of the high, dry, cold East Antarctic plateau and by the relatively warm, wetter weather systems that traverse inland from the West Antarctic ice sheet and Filchner-Ronne and Ross Ice Shelves. Synoptic heat- and moisture-bearing storm events reach the South Pole from the northwest Atlantic Weddell Sea and southwest Pacific Ross Sea [Hogan *et al.*, 1982; Harris, 1992; Nicolas and Bromwich, 2011]. The South Pole region typically receives dry continental, katabatic winds originating higher on the East Antarctic plateau, prevailing from 45°E, at 2–5 m s⁻¹ grid southwest across the region [Lazzara *et al.*, 2012]. The South Pole mean annual air temperature is -49°C, based on a 50 year surface climatology [Lazzara *et al.*, 2012]. Approximately 20 cm of snow falls per year around South Pole, equaling ~7–10 cm water equivalent per year [McConnell *et al.*, 1997; Mosley-Thompson *et al.*, 1999]. From the European Centre for Medium-Range Weather Forecasts reanalysis data, roughly half of South Pole snow accumulation is delivered from storms originating in the oceans off West Antarctica, and the remainder is from clear-sky, “diamond dust” snow [Radok and Lille, 1977]. Due to the cold temperatures in the South Pole region, fossil fuel combustion emissions precipitate rapidly and emission fallout remains localized [Brier *et al.*, 1998].

The seven measurement sites where spectra and samples were collected are mapped in Figure 1 and include (1) clean snow from the clean air sector, (2) a snow site upwind of generators, (3) snow less 0.5 km downwind of generators, and (4) snow on the aircraft runway entry/exit point, (5 and 6) aircraft taxiway/parking areas, and (7) aircraft fueling area. The seven sites receive relatively low annual snow accumulation, and the clean air sector and upwind of generator sample sites receive minimal snow disturbance. The downwind of generator area received continual fossil fuel emissions during the austral 2014–2015 season. The aircraft skiway, taxi, and fueling areas receive weekly intensive, direct fossil fuel emissions and potential thermal impacts during the austral summer when aircraft are parked with engines running for extended periods of time (nominally idle 45 min) [Brier *et al.*, 1998].

3. Methods

3.1. Field Spectroscopy

During the austral summer 2014–2015 season, field spectra were collected at the seven locations surrounding South Pole Station. Surface reflectance was measured with an Analytical Spectral Device (ASD) FieldSpec 4 Standard-Resolution spectroradiometer (colloquially “field spectrometer”) which measures the distribution of radiation in hyperspectral resolution from 350 to 2500 nm. The instrument was controlled by a laptop computer with ASD RS3 software [Analytical Spectral Devices Inc., 2011]. The spectral resolution of the instrument is 3 nm in the visible and near-infrared (VNIR) region (350–1000 nm) and 10 nm in the short-wave infrared (SWIR) region (1001–2500 nm) at full width half maximum; the spectra are resampled and splined to 1 nm resolution. The fiber optic cable of the field spectrometer contains 57 glass fibers: nineteen 100 μm fibers for



Figure 2. Field spectra collection (top) at spectral sample site 1, in the clean air sector on 7 December 2014 and (bottom) at spectral sample site 7 on the South Pole Station runway on 2 January 2015.

along with the bulk of the tripod setup, away from the Sun to avoid shadowing or interference with the measurement area. Figure 2 displays spectral sample collection setup in the clean air sector and aircraft runway sites.

For the sampling strategy, on each spectral measurement day, two areas within collection sites were sampled to measure snow diversity within the site. Spectra were collected in five snow and five calibration target acquisitions and repeated for sets of at least 100 spectra per sample area. Data represent multiple observations from a nominal summer season. During the 2014–2015 season, there were a few minor storms that deposited or redistributed snow slightly across the region. Our repeat spectral and sample collection measurements of the aircraft runway were aimed at considering this freshening of the runway snow surface and capturing the range of spectral response and impurity content found on surface snow during a typical summer season in the domain of the largest fossil fuel emission fallout. The sample collection attributes are detailed in Table 1.

The hemispherical-directional reflectance factor (HDRF) was calculated [Nicodemus *et al.*, 1977; Martonchik *et al.*, 2000; Schaepman-Strub *et al.*, 2006]. Due to FieldSpec instrument variability from the 57 optical fibers in three detectors and single spectra collection variability, resulting from atmospheric, illumination, and angular response variability, repeat target to calibrated panel reflectance factors were averaged to form representative HDRF (here after referred to simply as spectral reflectance). Table 2 lists the number of

VNIR, nineteen 200 μm fibers for SWIR1 (1001–1830 nm), and nineteen 200 μm fibers for SWIR2 (1831–2500 nm), which are randomly distributed in a fiber optic bundle. For our measurements, spectra were set to be the average of 25 scans, where data are collected at 0.2 s per scan.

The spectral measurement setup is described as follows. Spectra were collected in nadir, 25° field of view, on clear-sky days, within 2 h of local solar noon (10:00 A.M. to 2:00 P.M. LT) to ensure high, near-constant incident solar radiation flux during measurement. Snow with flat, near-homogenous surfaces and visually even snow grain distributions was targeted for measurement. A tripod positioned approximately 120 cm above the snow surface, with a mounted steel rod to extend the fiber optic cable, was used to collect spectra equating to an ~ 53 cm diameter ground field of view. A calibrated, lossless, diffuse Spectralon reflectance standard panel (25 cm^2) was positioned on a second tripod 90 cm above the snow surface. Bubble levels were used on the tripods and the fiber optic steel rod to ensure nadir, horizontal surface view angles. During all measurements, the operator wore all black outer clothing and was positioned,

Table 1. List of the Field Spectroscopy and Snow Sample Collection Attributes, With Snow Classifications After Fierz *et al.* [2009] (Where Snow Hardness of 2 = Soft, 4 = Hard, Snow Roughness of rsm = Smooth, rrd = Sastrugi, Erosion Features)

Sample ID	Location	Date	Data Collected	Snow Hardness	Snow Roughness
1a, 1b, 1c, 1d	Clean air sector	12-7-14	100 Field spectra, 4 snow samples	2	rsm
2a, 2b, 2c, 2d	Upwind of generator	12-18-14	200 Field spectra, 4 snow samples	2	rrd, slight sastrugi
3a, 3b, 3c, 3d	Downwind of generator	12-18-14	220 Field spectra, 4 snow samples	2	rsm
4a, 4b, 4c, 4d	Start of runway, aircraft landing	12-12-14	110 Field spectra, 4 snow samples	4	rrd, wind blown erosion features
5a, 5b, 5c, 5d	End of runway, aircraft parking	12-11-14	100 Field spectra, 4 snow samples	4	rrd, vehicular disturbed snow
6a, 6b, 6c, 6d	End of runway, aircraft parking	12-14-14	200 Field spectra, 4 snow samples	4	rrd, slight erosion
7a, 7b, 7c, 7d	Runway apron, aircraft fueling	1-2-15	200 Field spectra, 4 snow samples	4	rrd, slight erosion

spectral target to calibrated panel pairs used in creating each spectral reflectance average, as well as the average full spectrum standard deviation. Optical fiber checks were performed before and after each set of field measurements while at South Pole Station, to confirm all 57 VNIR, SWIR1, and SWIR2 optical fibers maintained signal strength. The field spectrometer was checked for optical calibration prior to and after field deployment, showing excellent repeatability (within 0.1% on average from 350 to 2500 nm). The averaging, optical fiber checks and optical calibration provide information on spectral acquisitions stability and precision. These spectral reflectance measurements can be compared with, and included in, standard

Table 2. Parts Per Billion Concentrations of BC and Trace Elements Measured in this Study and Compared To Other South Pole Area Snow Chemistry Studies^a

Sample	BC	Na	Mg	Al	S	Ca	Cr	Mn	Fe	Co	Cu	Zn	As	Cd	Ba	Pb
1a	0.14	27	2.8	2.1	9.5	220	0.026	0.083	0.41	0.0059	0.38	1.2	0.0024	0.012	0.14	0.014
1b	0.16	22	2.7	2.8	18	99	0.013	0.063	0.19	0.0028	0.15	0.84	0.0017	0.0050	0.062	0.026
1c	0.39	30	2.6	2.0	20	110	0.014	0.052	0.25	0.0031	0.50	0.74	0.0016	0.0051	0.072	0.017
1d	0.36	16	3.4	4.6	16	150	0.023	0.10	2.9	0.0019	0.93	0.69	0.0041	0.0028	0.99	0.058
2a	0.76	87	3.5	0.35	36	270	0.032	0.072	0.40	0.0020	0.13	1.2	0.0014	0.0089	0.11	0.0044
2b	0.27	97	2.7	0.57	17	75	0.029	0.043	0.26	0.0016	0.20	0.63	0.00045	0.0054	0.12	0.014
2c	0.32	59	3.3	0.94	24	210	0.042	0.052	0.52	0.0034	0.52	1.1	0.0017	0.0070	0.085	0.0087
2d	0.80	33	3.0	0.71	31	260	0.032	0.075	0.51	0.0037	0.13	0.84	0.0019	0.0095	0.076	0.0053
3a	6.3	44	4.4	4.4	38	270	0.057	0.24	3.1	0.0055	1.5	1.3	0.0036	0.021	0.10	0.062
3b	6.6	34	9.4	16	27	120	0.22	0.42	31	0.012	1.7	0.95	0.013	0.017	0.31	0.11
3c	2.6	22	5.8	7.8	22	170	0.098	0.24	13	0.0054	0.78	1.5	0.0061	0.0077	0.098	0.055
3d	4.2	24	5.9	12	26	170	0.15	0.39	25	0.0076	0.57	1.4	0.0088	0.048	0.17	0.090
4a	6.7	28	3.3	3.8	25	300	0.083	0.22	12	0.0059	1.6	1.0	0.0066	0.045	0.57	0.056
4b	130	19	3.0	25	21	85	0.096	0.15	9.6	0.0033	2.2	0.95	0.0080	0.070	0.49	0.052
4c	13	49	5.7	5.5	36	380	0.16	0.23	13	0.0091	3.5	2.5	0.011	0.11	0.71	0.24
4d	16	39	4.6	6.3	36	170	0.16	0.17	13	0.0053	1.8	1.3	0.0092	0.16	0.33	0.074
5a	4000	49	10	24	610	180	0.88	1.6	180	0.26	120	5.1	0.030	6.1	3.3	6.2
5b	3300	42	9.5	26	540	95	1.2	1.4	120	0.23	20	3.1	0.027	0.19	2.3	2.9
5c	960	110	18	44	350	410	0.78	1.4	99	0.11	1.8	4.4	0.028	0.11	1.8	0.25
5d	970	56	12	28	400	180	0.68	1.5	160	0.12	3.6	4.4	0.028	1.3	2.8	0.38
6a	4300	160	16	26	380	530	0.69	1.3	140	0.34	5.2	4.4	0.031	0.18	2.4	0.46
6b	3400	100	14	42	630	280	0.80	2.1	200	0.56	17	4.5	0.036	0.33	2.6	1.2
6c	1800	48	7.2	21	110	120	0.13	0.64	55	0.043	0.87	1.3	0.015	0.037	0.86	0.097
6d	490	34	8.6	14	110	170	0.15	0.50	41	0.028	0.86	1.2	0.014	0.054	4.2	0.11
7a	510	43	27	42	210	140	1.0	2.1	130	0.095	3.1	3.3	0.021	0.39	1.8	0.19
7b	2400	26	7.5	16	240	73	0.46	1.5	150	0.086	2.7	2.5	0.023	0.67	2.0	0.24
7c	6600	130	39	53	1200	570	1.9	6.2	660	0.52	14	6.3	0.082	0.49	22	1.2
7d	7000	47	13	24	840	140	1.0	2.9	280	0.34	4.5	3.0	0.047	0.66	5.3	1.5
Boutron [1982]			1.1	0.66		0.62		0.0063	0.39		0.025	0.072		0.010		0.028
Boutron and Patterson [1987]																0.0063
Warren and Clarke [1990]	<0.5															
Ferris <i>et al.</i> [2011]		~10	<3		(SO ₄ 50)											
Dixon <i>et al.</i> [2013]		6.6	6.5	2.1	6.6	2.3	0.012	0.025	0.90	0.023			0.0035	0.0041	0.019	0.012
Korotkikh <i>et al.</i> [2014]															0.296	

^aBoutron [1982], Boutron and Patterson [1987], Warren and Clarke [1990], and Ferris *et al.* [2011] measurements were from snow collected near South Pole station. Dixon *et al.* [2013] and Korotkikh *et al.* [2014] snow samples are from the ITASE 2002–2006 site near South Pole.

spectral reflectance libraries [e.g., Clark, 1999] and used as references in identification of remotely sensed elemental, mineralogic, and molecular compositions.

3.2. Snow Sample Collection

Immediately after spectral reflectance measurements were conducted, snow samples were gathered. A total of 28 surface snow samples were collected at the seven field spectroscopy sites (detailed in Table 1). Surface snow was collected at each spectral sample area, representing an approximate 30 cm × 30 cm area and the upper 3 cm of snow. Snow samples were collected in duplicate for each targeted field spectroscopy area and labeled by sample identification (ID). For each site, sample IDs a and b represent area 1, and sample IDs c and d represent area 2. New polypropylene gloves were worn during each snow sample collection. Surface snow samples were placed in clean Whirl-Pak bags, double bagged, and kept frozen in temperature-controlled, dark environments until measured in the labs as described in sections 3.6 and 3.7.

3.3. Grain Size and Albedo

Optical grain radius (OGR) is an important factor in modeling snow albedo as it determines reflectance in the near infrared and mainly controls clean snow broadband albedo. Snow spectral reflectance was inverted for OGR using the ice absorption feature centered at 1030 nm by best matching the integral across the continuum-normalized spectrum (950 to 1090 nm) to those for theoretical OGRs contained within a look-up table [Nolin and Dozier, 2000]. The look-up table is generated through repetitive runs of the Discrete Ordinates Radiative Transfer Program (DISORT) [Stamnes et al., 1988], an algorithm which simulates the radiative transfer through a homogenous snowpack composed of spherical grains of pure ice of a given grain size and specified illumination and reflection geometry. Uncertainty in the method is ±10–50 μm for grain sizes between 50 and 900 μm [Nolin and Dozier, 2000]. For simplicity, we will refer to OGR hereafter as grain size.

Similar to the methodology to convert snow reflectance to albedo from remote sensing [e.g., Painter et al., 2013], measured snow reflectance was converted to albedo via the spectral application of the anisotropy factor, which is the relationship between modeled reflectance and albedo for the same grain size and illumination/viewing angle. We note that this requires the assumption that the scalars between albedo and reflectance are not impacted by impurity content, an assumption that has not been tested. Clear-sky spectral irradiance for Antarctic summer was modeled with the Santa Barbara DISORT Atmospheric Radiative Transfer model (SBDART) [Ricchiuzzi et al., 1998]. Daily variation in irradiance was accounted for by scaling modeled irradiance such that its spectral integration matched measured broadband irradiance measured at NOAA’s South Pole Observatory (<http://www.esrl.noaa.gov/gmd/obop/spo/>). From measured albedo and SBDART irradiance spectrally weighted albedo between 350 and 750 nm (visible), 750 and 2500 nm (near/shortwave infrared), and 350 and 2500 nm (broadband) was calculated by dividing the product of the summation of irradiance and albedo by the summation of irradiance, i.e., for broadband albedo (equation (1)).

$$\alpha = \frac{\sum_{\lambda=0.35 \mu\text{m}}^{2.5 \mu\text{m}} I * \alpha_{\text{LAP}} \Delta\lambda}{\sum_{\lambda=0.35 \mu\text{m}}^{2.5 \mu\text{m}} I \Delta\lambda} \quad (1)$$

where I is scaled spectral irradiance at the given solar zenith angle, α_{LAP} is the albedo at the same solar zenith angle, and note that λ is the wavelength in micrometer.

3.4. Radiative Transfer Modeling

The Snow, Ice, and Aerosol Radiation (SNICAR) model (<http://snow.engin.umich.edu/>) [Flanner et al., 2007, 2009] was used to model spectral albedo of snow at South Pole collection sites given meteorological and measured parameters. The SNICAR model, developed after the two-stream radiative transfer solution of Toon et al. [1989], computes multiple scattering and reflectance from snow and impurity mixtures across 470 bands (300 to 5000 nm) at 10 nm resolution. In addition to solar zenith angle, input fields include effective (optical) snow grain size, snowpack density, snow and firn thickness, albedo of underlying ground, and impurity concentrations, which can be specified for uncoated and sulfate-coated BC, dust concentrations in four size bins, and volcanic ash. For albedo modeled in this study, the solar zenith angle input corresponded to time of snow reflectance measurement, the optical grain size input was that retrieved from the measured

snow reflectance, snow density was set to 350 kg m^{-3} [Giovinetto and Schwerdtfeger, 1965; Jouzel et al., 1983], and snow thickness was set to 120 m [Kuivinen et al., 1982].

Albedo was modeled with SNICAR for snow measured at South Pole sample sites, where impurity concentrations measured were used for model input. Measured Al was used to approximate dust content in snow, as it is a major constituent of dust reaching Antarctica [Planchon et al., 2002; Schwanck et al., 2016] and was found to be minimally enriched compared to dominant crustal elements measured. Antarctic plateau Al snow concentrations have been found to be predominantly in particulate fraction, bound to refractory phases (e.g., oxides) yielding acid dissolvable fractions at $\sim 5\%$ [Grotti et al., 2011]. Therefore, Al measured from snow samples in our study was estimated to represent 5% of total dust concentration and divided by two as the principal Al component found in crustal dust is Al_2O_3 [Wedepohl, 1995]. Radiative forcing was then estimated by taking the summation of the product of spectral irradiance and the difference between the spectrally weighted dust/BC albedo and clean snow albedo, which represents the enhanced surface absorption due to impurity content, for broadband wavelengths (equation (2)).

$$\text{RF} = \sum_{\lambda=0.35\mu\text{m}}^{2.5\mu\text{m}} I^*(\Delta\alpha)\Delta\lambda \quad (2)$$

where $\Delta\alpha = \alpha_{\text{clean}} - \alpha_{\text{LAP}}$, which is the difference between clean and impurity containing snow albedo at the same solar zenith angle, grain size, and density.

3.5. Optical Microscopy

A Nikon Measuring Microscope, model MM-40, was used to take optical microscopy digital images of the South Pole snow samples in cold laboratory conditions (-10°C) within the Snow and Ice Research Facility at NASA Goddard Space Flight Center in Greenbelt, Maryland. Bright field illumination was used with 2.5X and 5X magnification objectives to illuminate and image the snow grains and the larger visible LAPs [Pluta, 1988]. The optical microscopy imaging provided a qualitative estimate of snow grain size and LAP impact on the snow and the variability of these qualities among the seven site samples.

3.6. Black Carbon Measurement

The BC concentrations in the South Pole surface samples were measured using a Single Particle Soot Photometer coupled with a CETAC U-5000-AT+ nebulizer at Central Washington University. The SP2 uses laser-induced incandescence to measure the mass of refractory BC in single particles [Stephens et al., 2003; Schwarz et al., 2006]. The SP2 measures refractory BC; however, for simplicity we use the term BC. Monitoring of liquid sample flow rate pumped into the nebulizer, fraction of liquid sample nebulized, and purge air flow rate allows BC mass concentrations in the liquid sample to be determined. Because BC is not nebulized with 100% efficiency, Aquadag standards were used to correct the measured BC concentrations for BC losses that occur during nebulization. However, this standard correction does not address the size-dependent nebulization that occurs in the Cetac U-5000AT+ nor does it account for BC particles that are outside of the SP2 detection range (80–600 nm in this study). Thus, the measured BC concentrations reported herein represent lower limit values. Further details are provided in Wendl et al. [2014] and Kaspari et al. [2014].

To prepare for snow sample measurement, polypropylene (PP) sample vials were soaked in 15% trace metal-grade nitric acid for 1 week, triple rinsed with deionized water, soaked in deionized water another week, triple rinsed, and dried in a class-100 HEPA clean room. All samples were kept frozen until just prior to SP2 measurement. Snow samples were transferred from Whirl-Pak collection bags to 120 mL clean PP vials. Snow samples were then melted, upon which some vials became dark gray or black colored. This dark coloring on some vials likely indicated adhesion of BC onto the PP vial walls. Because of concerns that substantial BC was lost to the vial walls, high BC concentration snow samples 5a, 5b, 6a, 6b, 6c, 7b, 7c, and 7d were remeasured with new snow sample in nitric acid soaked, deionized water cleaned glass Pyrex vials which prevent adhesion to container walls. These high BC concentration samples were diluted with deionized water, sonicated, and diluted again to allow accurate measurement in the SP2. All samples were sonicated for 25 min and immediately analyzed while being stirred with a magnetic stir bar for BC concentration. Procedural blanks were used to characterize the instrument detection limit.

3.7. Trace Element Measurement

A Thermo Element 2 Inductively Coupled Plasma Mass Spectrometer (ICPMS) was used for trace element concentration measurement. The sample introduction system was an Elemental Scientific Apex with a 100 $\mu\text{L}/\text{min}$ self-aspirating Teflon Nebulizer. Trace elements Cd, Ba, Pb, and Cs were measured in low resolution; Mg, Al, S, Ca, Cr, Mn, Fe, Co, Cu, and Zn were measured in medium resolution and As was measured in high resolution. The ICPMS instrument was calibrated prior to sample analysis with standards intended to bracket the snow sample range. Snow samples containing concentrations that were beyond the ICPMS instrument calibration range were rerun with a higher concentration calibration applied. Standard reference material SLRS-5 (Environment Canada) was run to verify the ICPMS calibration.

Snow samples were acidified with trace metal-grade nitric acid such that the samples contained 1% nitric acid. Samples were mixed by shaking them after they were acidified and then several times while they were leaching for approximately 4 weeks. In the heaviest particulate concentration snow samples, some particulate material did not dissolve and very fine black material settled to the bottom of the container. Samples were not shaken immediately prior to ICPMS measurements as this fine material would plug parts of the instrument. The trace elements that were leached from the acid digestion into solution are included; however, measured trace elements likely do not represent a complete digestion of refractory particles. Deionized water blanks were measured and reflected very low trace element concentration contributions. Our acidification and leaching protocol was based on experiments conducted using WAIS Divide (West Antarctica) snow samples [Koffman *et al.*, 2014]. Cryospheric trace element ICPMS instrument measurement methods used in this study are further described in Osterberg *et al.* [2006].

4. Results

4.1. Optical Microscopy

Optical microscopy images of the span of clean to polluted runway snow samples showed significant differences. Bright field illumination at 5X magnification images revealed the clean air sector snow samples to be clear and contain smooth snow grain edges. In contrast, the increasing amount of particles in downwind of generator and aircraft runway samples resulted in snow grains which were progressively more opaque, darker in color, and concentrated with more fine particulate inclusions. Figure 3 demonstrates the contrast between clean air sector and runway snow samples, where the images have constant magnification and illumination applied. Observable snow grain sizes were found to be approximately 0.5 mm in diameter on average when measured in the laboratory, several months after sample collection. Thus, when measured spectrally in the field, snow grain sizes were likely smaller, as snow grains nominally grow with age [e.g., LaChapelle, 1969; Pirazzini *et al.*, 2015]. We note that observable snow grain size does not necessarily equate to optical snow grain size, which is the radius of the sphere that returns the same hemispherical flux.

4.2. Black Carbon Concentrations

The clean air sector and upwind from generator snow samples contained the lowest BC concentrations, averaging 0.26 ppb (parts per billion) and 0.54 ppb, respectively (Table 2 and Figure 4) and generally agree with the magnitude of BC found in previous South Pole area clean snow studies [e.g., Warren and Clarke, 1990]. Downwind from the generator and aircraft runway, BC concentrations were significantly higher, with BC sample area averages of 4.9 ppb (site 3), 41 ppb (site 4), 2300 ppb (site 5), 2500 ppb (site 6), and 4100 ppb (site 7), respectively. As expected, the heaviest BC concentrations were found in the aircraft landing, parking, and fueling areas where fossil fuel emissions are estimated to be strongest and transport distance shortest. Aircraft fueling sample site 7 contained the highest BC concentration of 6600 and 7000 ppb, in samples 7c and 7d, respectively. These BC concentrations also are likely to be lower than actual BC, due to the limitations of the SP2 detection range (80–600 nm).

BC concentrations measured are highest within 1 km of emission sources, and concentrations reduced with greater distances from emission source, agreeing with findings from previous emission fallout studies [e.g., Warren and Clarke, 1990; Warren *et al.*, 2006]. BC concentrations measured in aircraft runway snow sample sites 5–7 are comparable and/or higher (samples 5a, 5b, 6a, 6b, 7c, and 7d) than BC concentrations reported in other anthropogenically impacted BC on snow studies, (e.g., snow in Northern China of 1220 ppb BC,

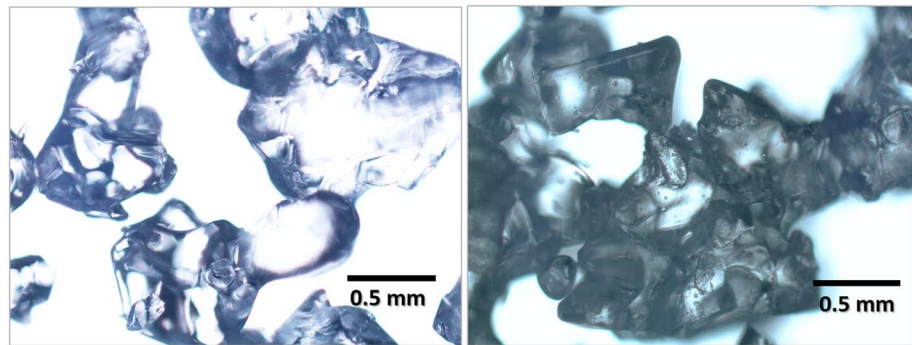


Figure 3. Bright field, 5X magnification optical microscopy images of snow grains collected in (left) the clean air sector, sample 1d and (right) South Pole aircraft runway, sample 7d.

reported in Wang *et al.* [2013] and snow near a coal mine in Svalbard with refractory BC 345 ppb, effective BC 4900 ppb, reported in Khan *et al.* [2017]).

4.3. Trace Element Concentrations

Significant increases in trace element concentrations were found for most elements from clean air sector and upwind of generator snow to downwind of generator and aircraft runway snow. Concentrations for each sample and element are listed in Table 2 and plotted in Figure 5. The major natural sources of particles to South Pole region come from crustal dust, sea salts, and intermittently volcanic ash. Trace elements measured from our clean air sector snow samples generally agree with previously reported values (Table 2); however, aircraft runway trace element concentrations were significantly higher due to the anthropogenic fossil fuel combustion near South Pole.

To discern the snow sample trace elemental contribution from natural or anthropogenic source, crustal and oceanic Enrichment Factors (EF) (equations (3) and (4)) were calculated for each sample and element. EF provide a simple, robust means to evaluate measured sample elemental concentrations as compared to

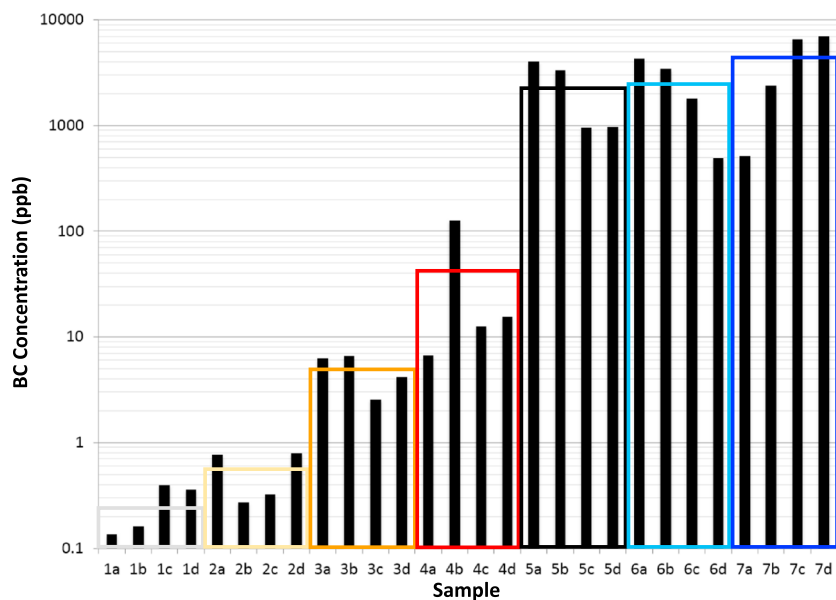


Figure 4. BC concentration (ppb) of 28 South Pole snow samples. Height of colored box corresponds with average BC concentration per sample site. The clean air sector displays the cleanest snow (1), followed by upwind of a science generator (2), and then progressively more polluted snow downwind of generator (3), and on the aircraft runway (4–7).

elemental abundances in standard reference materials. Enrichment factors greater than 10 indicate significant contribution from sources other than the reference material.

Crustal enrichment factors (EF_c) were calculated to assess the relative abundance of trace elements relative to Earth's upper continental crust. For this study, upper continental crust elemental abundances after *Wedepohl* [1995] were used as the standard reference material, and Cesium (Cs), an alkali metal with relatively low natural or anthropogenic emission sources, was used as the reference element.

$$EF_c = \frac{(X/Cs)_{\text{snow}}}{(X/Cs)_{\text{STD}}} \quad (3)$$

where " EF_c " corresponds to crustal enrichment factor of element " X ." $(X/Cs)_{\text{snow}}$ is the concentration ratio measured in the snow sample. $(X/Cs)_{\text{STD}}$ is the concentration ratio of the upper continental crust.

The EF_c determined deviations from crustal enrichment are listed as follows and displayed in Figure 5 (right). No crustal enrichment was found for Al. Minimal crustal enrichment was found for Mg and Mn. High enrichment relative to the crust was found for Fe and Ba in runway only snow samples. Significant enrichment relative to Earth's crust was found in all snow samples for S, Ca, Cr, Co, Cu, Zn, As, Cd, and Pb. Fossil fuel combustion is the primary suspected cause for S, Cr, Mn, Fe, Co, Cu, Zn, As, Cd, Ba, and Pb enrichment near South Pole; enrichment of these elements is indicative of anthropogenic fossil fuel emission particle deposition [*Vouk and Piver*, 1983; *Pacyna and Pacyna*, 2001].

Enrichment compared to oceanic water was also assessed, using Na as a reference element [e.g., *Dixon et al.*, 2013; *Schwanck et al.*, 2016] and the abundance of ocean water after *Huheey et al.* [1993].

$$EF_o = \frac{(X/Na)_{\text{snow}}}{(X/Na)_{\text{STD}}} \quad (4)$$

where " EF_o " corresponds to oceanic enrichment factor of element X . $(X/Na)_{\text{snow}}$ is the concentration ratio measured in the snow sample. $(X/Na)_{\text{STD}}$ is the concentration ratio of ocean water.

Mg showed no-to-negligible enrichment compared to oceanic water across the samples. S showed no consistent enrichment in clean air sector and upwind of generator snow, however, slight and strong enrichment in downwind of generator and aircraft runway samples, respectively. Other trace elements (Al, Ca, Cr, Mn, Fe, Co, Cu, Zn, As, Cd, Ba, and Pb) showed very strong enrichment compared to oceanic water in all snow samples.

Influence from crustal and marine natural processes was signaled by the concentration and enrichment patterns in Na, Mg, Al, and Ca in the snow samples. Sporadic, short duration (10–20 day) events are known to bring marine influenced, sea salt aerosol enrichment (e.g., Na, Mg, and Ca) to the South Pole region year round [*Tuncel et al.*, 1989]. Natural marine sourced Na, Mg, and Ca enrichment revealed near-stable values across all sample sites, with slightly higher EF in undisturbed snow areas (sites 1 and 2). Dust transport to South Pole has been found to be highest in the calmer meteorological conditions of austral summers [*Tuncel et al.*, 1989]. The relatively low concentration of Al in all samples likely represents crustal dust transport contributions to the ice sheet and less prevalent contributions from fossil fuel combustion. Sulfur is more volatile compared to nonreactive trace metals and can thus be more challenging to study provenance in snow [*Dibb*, 1996]. However, the cold, dry climate of South Pole lessens chemical reaction speed as compared to more temperate conditions. Sulfur was found to be heavily enriched relative to both crustal and ocean standards, especially in the runway snow samples. We hypothesize that fossil fuel emissions contribute significantly to the high S concentrations measured in aircraft runway snow samples, and the cold, dry climate of South Pole aids in preserving deposited S.

Overall, influence of natural processes, such as transport of sea salts, dust, and volcanic particles to South Pole snow, was minimal compared to the anthropogenic impacts. Annual aircraft emissions of particles at South Pole were estimated to be 820 kg, based on nominal flights to and from the station and the required engine idling time due to cold conditions and engine design [*Brier et al.*, 1998]. South Pole Station operations, including power generation, heating, water production, and equipment operation, are estimated to contribute another 1500 kg of particles to the atmosphere per year [*Brier et al.*, 1998]. The collective-estimated particle emissions, high-trace element concentrations measured, and high crustal and oceanic enrichment factors of

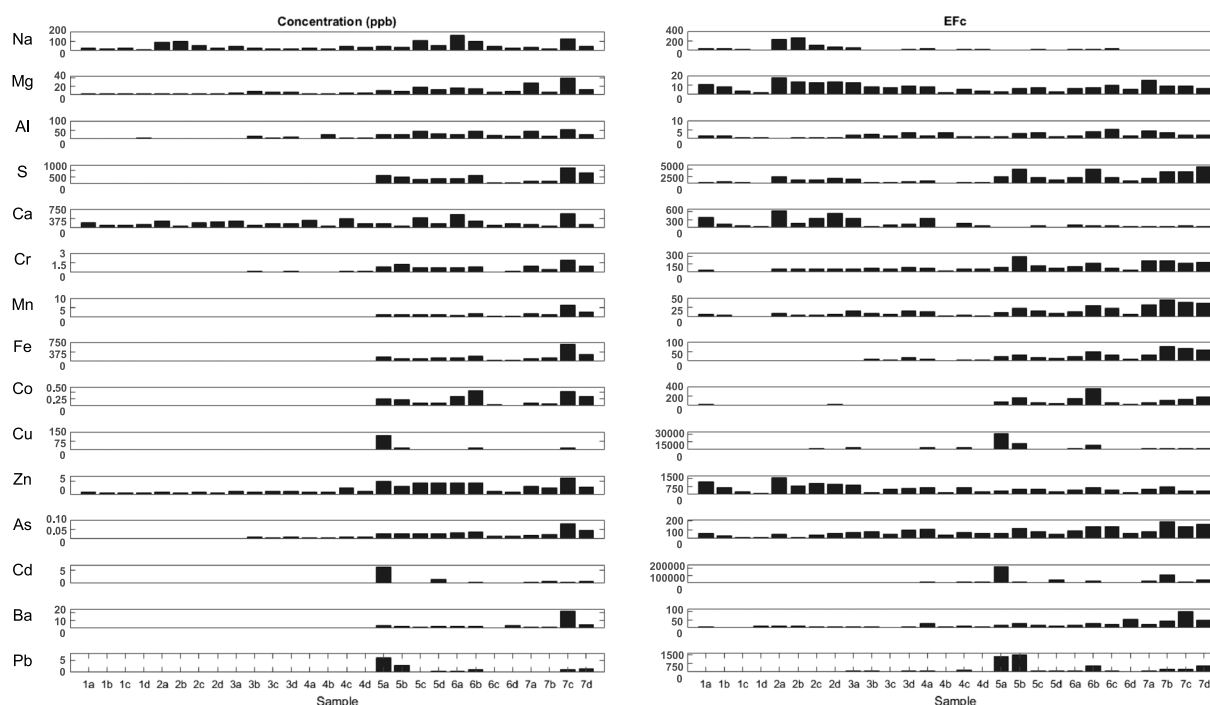


Figure 5. South Pole snow sample trace element concentrations (left) and crustal enrichment factors (right) show increasing abundance and enrichment of most trace elements in snow downwind of generators and on the aircraft runway.

S, Cr, Mn, Fe, Co, Cu, Zn, As, Cd, Ba, and Pb signal significant anthropogenic contribution to the snow from fossil fuel combustion.

4.4. Snow Spectroscopy and LAP Impact

LAPs have detectable impacts on snow spectral reflectance. South Pole area snow spectral reflectance displayed a gradient from high visible-SWIR reflectivity in the clean air sector snow to lower visible-SWIR reflectivity in the heavily contaminated aircraft runway snow as expected. Specifically, snow spectral reflectance in the clean air sector, with an average of 0.26 ppb BC, 16 ppb S, 0.94 ppb Fe, 0.019 ppb Cr, 0.075 ppb Mn, and 0.49 ppb Cu had an average of 30% higher visible-SWIR reflectance than the most polluted runway snow, with average 4100 ppb BC, 310 ppb Fe, 1.1 ppb Cr, 3.2 ppb Mn, 5.9 ppb Cu. Figure 6 demonstrates the spectral reflectance variability found within each sample site, at the two sampling areas, where the maximum and minimum spectral response per sample area is shown in semitransparent color, and the sample area average spectral reflectance shown in bold, solid lines. Table 3 lists the number of spectral pairs (snow/Spectralon) averaged for each sampling area and the average standard deviation of the spectral reflectance. The standard deviations of the full visible-SWIR reflectance measurements were well under 1%, translating to stable spectral acquisitions. All high-quality snow spectra results are presented in Figure 6, equating to a total of 380 snow spectra, 190 spectral pairs. Note that some snow spectra collected during the season are not presented due to pronounced anisotropic effects [see *Painter and Dozier, 2004*] noted in some spectra from site 1 with the fine-grained pristine snow and anisotropic effects and outside of solar noon returns for most spectra at sites 2 and 3.

For all high-quality snow spectra, characteristic snow absorption features were noted, including the higher visible reflectance and decrease in NIR and further in SWIR with local maxima at 1100, 1300, 1800, and 2200 nm (i.e., described in *O'Brien and Munis [1975]* and *Wiscombe and Warren [1980]*). Upon close inspection, atmospheric oxygen absorption can be seen at approximately 765 nm in many spectra. The SWIR absorption features found in snow spectra from approximately 1500–2100 nm may signal elevated hydrocarbons [*Clark, 1999*], which was not measured in this study, though a primary fossil fuel combustion by-product. Overall, the snow reflectance shape changed from site to site and to a lesser extent within the two sample areas per site.

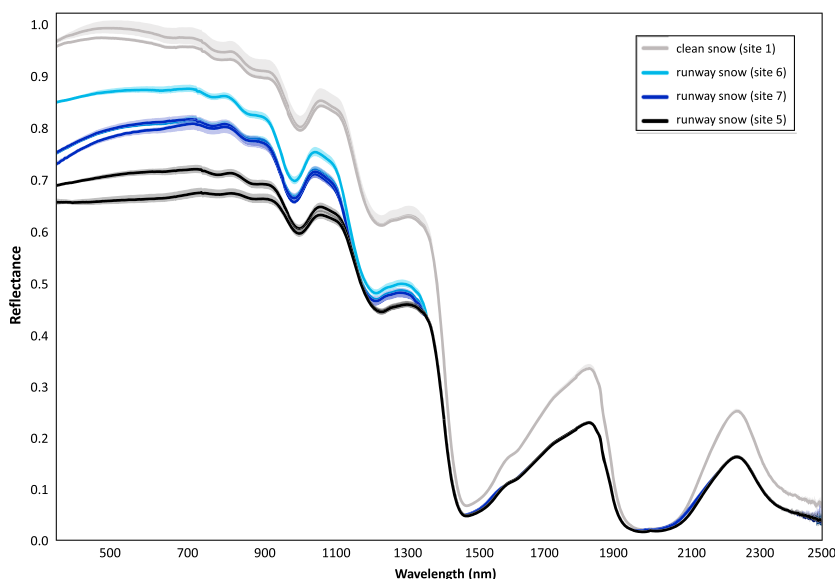


Figure 6. The range of spectral reflectance measured for clean air sector snow compared to the increasingly polluted runway snow is plotted by maximum, minimum (transparent upper and lower bounds), and average (solid line) for the two areas within each sample site.

The visible range of the spectrum provides a means to understand LAP composition. Spectral characterization of LAP continues to be studied. Particles are challenging to define spectrally due to component element charge, bond(s) and/or orientation in host matrix, all which can result in variations to absorption features. Snow reflectance changes from UV-near infrared are altered by organics, S, Fe, Cr, Mn, Cu, and BC concentrations. Specifically, organics are known to yield absorption features in UV, S at 280 and 400 nm; Fe at 440, 870, and 950 nm; Mn at 340, 370, 410, 450, and 550 nm; Cu at 800 nm; and Mg at 1000 nm [McClure, 1959; Hunt, 1977; Wiscombe and Warren, 1980; Clark, 1999; Gupta, 2003]. BC on snow is known to result in broad absorption in visible though 880 nm is often used as an open atmospheric measurement window with minimal contributions from other elements or compounds [Weingartner et al., 2003]. In our measured spectral reflectance, visible absorption was minor to negligible at site 1, and particularly strong for site 7, relative to sites 5 and 6. Correspondingly, site 7 snow samples displayed the highest concentrations of Fe, S, Cr, Mn, and Cu as detailed in results in section 4.3. The broad reduction of snow reflectance from visible to near infrared seen in the other snow reflectance curves (site 5 and 6) is attributed mainly to BC, which is near equally absorptive across the full solar spectrum [Wiscombe and Warren, 1980]. High concentrations of Cu and Pb may contribute to the reduced visible reflectance measured in site 5 spectra (i.e., if bonded to sulfur, see galena spectra Kokaly et al. [2017]). We note that specific elements are likely present on snow in mineralogic grains, salts, or molecular compounds; hence, specific absorption features are difficult to discern with this first step. Follow-on work will be targeted on LAP component mineralogy, laboratory spectra, and/or further computational methods. We estimate that snow grain size did not contribute significantly to the spectral reflectance differences measured in sites 5, 6, and 7 as there was minimal variation via quantitative retrievals (~150 μm)

Table 3. List of the Spectra Quantity and Statistics for the Most Reflective Clean Air Sector Snow (Site 1) and Progressively Less Reflective Aircraft Runway Snow (Sites 6, 7, and 5) as Plotted in Figure 6

Site	Sample Area	Number of Spectral Pairs	Average Standard Deviation
1	1	5	0.0018
	2	15	0.0081
6	1	20	0.0029
	2	30	0.0027
7	1	20	0.0032
	2	50	0.0042
5	1	25	0.0030
	2	25	0.0037

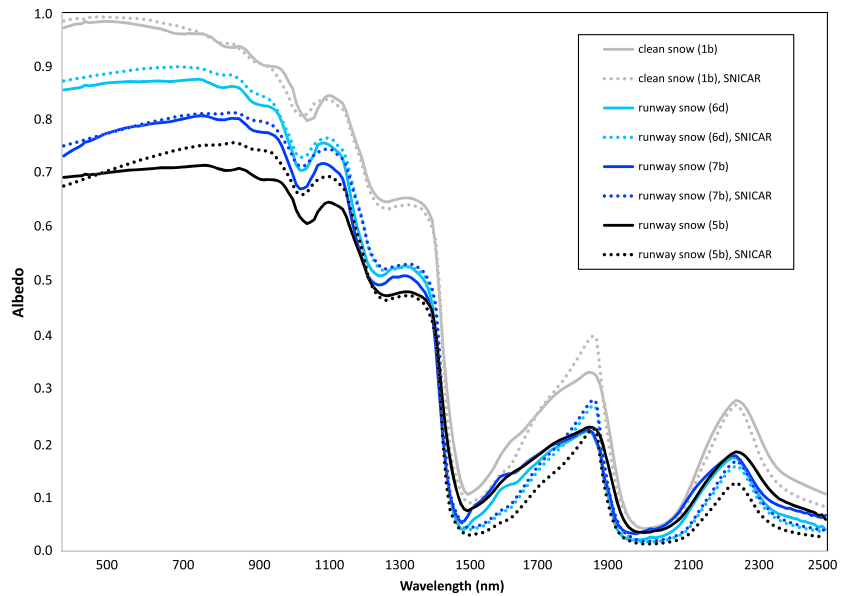


Figure 7. South Pole measured snow albedo (solid lines) compared with SNICAR modeled snow albedo (dashed lines).

and qualitative imaging microscopy (site 5 measured very slightly higher snow grain size via retrievals as detailed in the following section). Thus, other factors constant (illumination angle and setup), we find that the strong visible-absorbing elements are likely contributing to the enhanced absorption measured from 365 to 1000 nm.

4.5. Measured and Modeled Snow Albedo

This section provides an overview of the South Pole snow measured and modeled albedo, related variations in the retrieved snow grain size, broadband albedo, and radiative forcing. Comparison between measured albedo (estimated from reflectance measurements) and modeled albedo (SNICAR) is shown in Figure 7. Measured broadband (visible through shortwave infrared) albedos were highest for the clean snow site 1 at 0.85. Aircraft runway snow broadband albedos were 0.75 for site 6, 0.69 for site 7, and 0.62 for site 5 (Table 4). Retrieved snow grain sizes ranged from 67.8 μm (site 1) to 179 μm (site 5) for the clean and most contaminated runway site, respectively. The other two runway sites had similar grain sizes of ~150 μm. We found that snow sample sites with higher BC and trace element concentrations had lower broadband albedo, and larger snow grain sizes, relative to the cleaner site. These findings affirm both the general understanding of LAPs impacts on snow and previous studies and the reduction of spectral albedo or reflectance with increasing LAPs concentration (e.g., laboratory [Hadley and Kirchstetter, 2012]; in situ [Casey et al., 2012; Negi et al., 2015; Di Mauro et al., 2015]). We note that the larger grain sizes and lower NIR reflectance exhibited by aircraft runway snow could be due to compaction and higher local surface temperatures from parked or slowly moving aircraft in addition to enhanced grain growth related to LAPs radiative forcing.

There is some uncertainty in the albedo comparison analyses given that SNICAR does not model observed albedo perfectly. The average measured to modeled snow albedo differences ranged from +0.03 to -0.001 for sites 5 and 7, respectively, and were 0.01 on average. This can be translated to a reflected solar

Table 4. Measured Visible, Near Infrared, Broadband Albedo, and Radiative Forcing for the Clean Air Sector Snow and Aircraft Runway Snow Sample Areas in Order of Progressively Lower Albedo and Higher Radiative Forcing

Spectral Sample Area	Broadband Albedo: Visible (365–750 nm)	NIR-SWIR (750–2500 nm)	Visible-SWIR (365–2500 nm)	Radiative Forcing (W m ⁻²)
1-1	0.98	0.68	0.85	0.20
6-2	0.87	0.59	0.75	23
7-1	0.78	0.56	0.69	46
5-1	0.71	0.51	0.62	69

flux error, by applying measured and modeled albedo to the corresponding modeled spectral irradiance. The solar flux error here was quite low, ranging from $+2.18 \text{ W m}^{-2}$ to -2.5 W m^{-2} for sites 5 and 7, and was 0.02 W m^{-2} on average. This shows that in general SNICAR is able to model the reflectance of relatively clean snow and snow containing impurities well and that the uncertainty in radiative forcing due to modeling is low ($\pm 2.5 \text{ W m}^{-2}$). In this case, the least well modeled reflectance shape was across the visible wavelengths for site 5, which could be due to uncertainty in inputs, or optical property representation of impurities within the model. Currently, SNICAR uses a single mass absorption cross section for BC and general "global mean" dust optical properties (based on a mixture of quartz, limestone, montmorillonite, illite, and hematite) [Flanner *et al.*, 2007]. Recent work has shown that the model performance is improved when those optical properties are updated with those of deposited impurities [Skiles *et al.*, 2016]. Variations in spectral absorption due to specific mineralogic, elemental, or molecular constituents yield differing albedo. Further improvements to LAPs modeled albedo addressing these specific elemental and mineralogic constituent absorption characteristics are recommended.

4.6. Radiative Forcing

Radiative forcing was calculated for the four sites plotted in Figure 7. This radiative forcing represents the difference in absorption between impurity laden and pure snow for the same solar illumination, grain size, and density and therefore represents the direct impact due to LAPs (decrease in albedo) and does not represent the indirect impact due to LAPs (enhanced grain growth). From low to high BC concentrations corresponding instantaneous RF values were $<1 \text{ W m}^{-2}$ at site 1, 23 W m^{-2} at site 6, 46 W m^{-2} at site 7, and 69 W m^{-2} at site 5. For context, relative to clean snow and for an irradiance of 450 W m^{-2} , the snow at site 5 is absorbing $\sim 15\%$ more solar radiation due to the presence of LAPs, which has implications for local snow processes around the South Pole Station, and other snow regions exposed to fossil fuel emission deposition.

There are no other studies in Antarctica that we are aware of that have retrieved radiative forcing from spectral albedo measured and modeled from retrieved grain size and sampled LAP concentrations. There are other studies from midlatitude mountain sites, where due to proximity to LAP sources, we would expect radiative forcing to be higher. On the Mera Glacier (south slope of the Himalaya), Kaspari *et al.* [2014] found instantaneous radiative forcings from 75 W m^{-2} , for a BC concentration 258 ppb, up to 535 W m^{-2} , for a BC concentration of 1290 ppb and dust concentration of 9.3 parts per trillion (ppt). On Snow Dome, Mount Olympus, WA, Kaspari *et al.* [2015] found that the summer surface radiative forcing by dust and BC increased from $37\text{--}53 \text{ W m}^{-2}$ in 2011 to $112\text{--}149 \text{ W m}^{-2}$ in summer 2012, which was attributed to deposition of LAPs by a forest fire. Skiles [2014] presented a continuous time series of radiative forcing by dust and BC during ablation in the San Juan Mountains, CO, and found that radiative forcing ranged from 0.25 W m^{-2} for relatively clean snow to 525 W m^{-2} for snow heavily contaminated by dust. We note that in all of these studies both dust and BC concentrations were used to quantify radiative forcing, and in all instances dust dominated the radiative forcing signal, which is not the case for this study.

5. Conclusions

We found that there is a significant, localized impact on snow albedo reduction on the South Pole Station aircraft runway due to fossil fuel emission deposition. Light-absorbing particles lowered broadband snow albedo from 0.85 to 0.62 in the heaviest contaminated snow and resulted in radiative forcing up to $\sim 70 \text{ W m}^{-2}$. Full visible-SWIR spectrum snow reflectance was reduced 30% on average from the clean air sector snow to most polluted runway snow. This study provides the first comprehensive observational data set of snow reflectance, snow albedo, radiative forcing, black carbon, and trace element compositions of heavy pollution laden snow at South Pole, Antarctica. To our knowledge, previous studies have not had the analytical chemistry trace element and BC results coupled with spectroscopy and radiative impacts. The analytical chemistry and spectroscopy coincident data yield more accurate, precise understanding of surface composition. Surface composition is only qualitatively gleaned from remote sensing tools alone. LAPs deposited on snow were measured at seven locations of varying degrees of pollutant magnitude at South Pole during the 2014–2015 austral summer, and we found upper limit polluted snow concentrations to be 7000 ppb BC, 1200 ppb S, 660 ppb Fe, 1.9 ppb Cr, 6.2 ppb Mn, 120 ppb Cu, 6.3 ppb Zn, 82 ppt As, 6.1 ppb Cd, 22 ppb Ba, and 6.2 ppb Pb.

Our study provides a first step of spectrally resolving BC and trace element influence on snow reflectance from 350 to 2500 nm, given the analytical chemistry results. Measured snow albedo was compared to modeled snow albedo for clean snow and increasingly polluted snow, and the greatest disparities are suspected to be due to specific trace metal elemental and BC abundances. Follow-on work will further inspect LAP composition via laboratory and/or spectroscopic methods [e.g., Hadley and Kirchstetter, 2012; Kokaly, 2011]. Further research on fossil fuel and jet-propulsion fuel combustion emissions particle composition is highly recommended. We suggest that snow albedo models further refine elemental, molecular, and mineralogical absorption feature capabilities for accurately estimating high LAPs concentrations. Currently, many snow albedo models use generalized impurity categories (e.g., one dust type). Dust and particle types vary greatly depending on natural and anthropogenic LAP sources unique to the local environment. This study may provide a data set to explore albedo model impurity parameterizations.

There are also implications for other high albedo areas impacted by heavy fossil fuel emissions, namely, other cryospheric aircraft runways (McMurdo, Antarctica and Summit, Greenland) and cryosphere or desert mining and oil recovery facilities (Asia, Arctic, and Middle East). If pollution sources are strong and steady, albedo on large spatial scales can be affected. We recommend follow-on studies to further quantify fossil fuel combustion emissions and surface transformation at LAP-impacted locations. The reduction of surface albedo due to fossil fuel combustion and similar natural or anthropogenic albedo reductions can have significant regional radiative energy balance ramifications. Over snow, increasing LAP deposition can decrease snow albedo and enhance snow grain metamorphosis and/or melt and contribute to snow albedo feedback.

Spectral absorption features are key to improving not only in situ but also airborne and satellite snow remote sensing studies of cryospheric areas affected by LAPs. It has been proven that higher concentrations of impurities on snow and ice can be resolved and characterized via airborne and satellite remote sensing [e.g., Zege et al., 2008; Gleeson et al., 2010; Zege et al., 2011; Casey et al., 2012; Casey and Käbb, 2012; Painter et al., 2012, 2013; Seidel et al., 2016]. This study may be used to understand spectral response over snow with similar magnitudes of impurity concentrations (i.e., <1–3000 ppb BC, 9.5–1200 ppb S, and 0.19–660 ppb Fe). Further in situ, airborne, and satellite remote sensing spectral studies are recommended for areas of high particulate loading to cryospheric surfaces, such as near-natural volcanic, dust, biological, carbon, or anthropogenic emission sources, to improve LAPs on snow and ice magnitude and composition characterization capabilities and measure radiative impacts and surface albedo changes over time. Improved understanding of particle impacts on cryospheric surfaces is crucial to expanding our understanding of air-snow interactions and reducing uncertainties in projecting ice mass balance, sea level rise, and Earth's radiative energy balance.

Acknowledgments

This study was funded by the NASA GSFC Cryospheric Sciences Laboratory, via the ESSIC Cooperative Agreement. All surface snow black carbon and trace element concentration data used in this study are published within the article. Snow spectral data are available upon request (kimberly.a.casey@nasa.gov). We thank Tom Neumann, Leah Street and logistic support personnel at South Pole Station for sampling coordination assistance. We acknowledge Stan Scott at NASA GSFC for allowing use of the microscope and Adam Greeley with help in microscope set up and imaging. Finally, we thank three anonymous reviewers for their thoughtful comments. Kimberly Casey initiated, planned, and conducted the field study at South Pole, processed the spectral data and analytical chemistry results, and wrote the manuscript. Susan Kaspari processed samples for black carbon and helped edit the manuscript. S. McKenzie Skiles processed reflectance to retrieve grain size and modeled irradiance, albedo, and radiative forcing and contributed to the manuscript. Karl Kreutz and Mike Handley processed samples for trace elements and helped edit the manuscript.

References

- Analytical Spectral Devices Inc. (2011), Field Spec 4 User Manual, ASD Document 600979, Rev. A.
- Barrie, L. A. (1996), Occurrence and trends of pollution in the Arctic troposphere, in *Chemical Exchange Between the Atmosphere and Polar Snow*, edited by E. W. Wolff and R. C. Bales, pp. 91–129, Springer, New York.
- Bergin, M. H., E. A. Meyerson, J. E. Dibb, and P. A. Mayewski (1998), Relationship between continuous aerosol measurement and firn core chemistry over a 10-year period at the South Pole, *Geophys. Res. Lett.*, *25*, 1189–1192, doi:10.1029/98GL00854.
- Bodhaine, B. A., J. J. Deluisi, and J. M. Harris (1986), Aerosol measurements at the South Pole, *Tellus*, *38B*(3–4), 223–235.
- Bond, T. C., and R. W. Bergstrom (2006), Light absorption by carbonaceous particles: An investigative review, *Aerosol Sci. Technol.*, *40*(1), 27–67.
- Boutron, C. (1982), Atmospheric trace metals in the snow layers deposited at the South Pole from 1928 to 1977, *Atmos. Environ.*, *16*(10), 2451–2459.
- Boutron, C. F., and C. C. Patterson (1987), Relative levels of natural and anthropogenic lead in recent Antarctic snow, *J. Geophys. Res.*, *92*, 8454–8464, doi:10.1029/JD092iD07p08454.
- Boutron, C. F., and E. W. Wolff (1989), Heavy metal and sulphur emissions to the atmosphere from human activities in Antarctica, *Atmos. Environ.*, *23*(8), 1669–1675.
- Brier, F., R. Cunningham, J. Jatko, A. Jung, P. Karasik, and J. Maier (1998), *Modernization of the Amundsen-Scott South Pole Station Antarctica, Final Environmental Impact Statement*, 416 pp., Office of Polar Programs, Natl. Sci. Foundation, Arlington, Va.
- Casey, K. A., and A. Käbb (2012), Estimation of supraglacial dust and debris geochemical composition via satellite reflectance and emissivity, *Remote Sens.*, *4*(9), 2554–2575.
- Casey, K. A., A. Käbb, and D. I. Benn (2012), Geochemical characterization of supraglacial debris via in situ and optical remote sensing methods: A case study in Khumbu Himalaya, Nepal, *Cryosphere*, *6*, 85–100.
- Clark, R. N. (1999), Chapter 1: Spectroscopy of rocks and minerals, and principles of spectroscopy, in *Manual of Remote Sensing*, vol. 3, *Remote Sens. for the Earth Sci.*, edited by A. N. Rencz, pp. 3–58, John Wiley, New York.
- Dibb, J. (1996), *Overview of Field Data on the Deposition of Aerosol-Associated Species to the Surface of Snow of Polar Glaciers, Particularly Recent Work in Greenland, Chemical Exchange Between the Atmosphere and Polar Snow*, edited by E. W. Wolff and R. C. Bales, pp. 249–274, Springer, Berlin.

- Dixon, D. A., P. A. Mayewski, E. Korotkikh, S. B. Sneed, M. J. Handley, D. S. Introne, and T. A. Scambos (2013), Variations in snow and firn chemistry along US ITASE traverses and the effect of surface glazing, *Cryosphere*, *7*, 515–535, doi:10.5194/tc-7-515-2013.
- Di Mauro, B., F. Fava, L. Ferrero, R. Garzonio, G. Baccolo, B. Delmonte, and R. Colombo (2015), Mineral dust impact on snow radiative properties in the European Alps combining ground, UAV, and satellite observations, *J. Geophys. Res. Atmos.*, *120*, 6080–6097, doi:10.1002/2015JD023287.
- Doherty, S. J., T. C. Grenfell, S. Forsström, D. L. Hegg, R. E. Brandt, and S. G. Warren (2013), Observed vertical redistribution of black carbon and other insoluble light-absorbing particles in melting snow, *J. Geophys. Res. Atmos.*, *118*, 5553–5569, doi:10.1002/jgrd.50235.
- Ferris, D. G., J. Cole-Dai, A. R. Reyes, and D. M. Budner (2011), South Pole ice core record of explosive volcanic eruptions in the first and second millennia A.D. and evidence of a large eruption in the tropics around 535 A.D., *J. Geophys. Res.*, *116*, D17308, doi:10.1029/2011JD015916.
- Fierz, C., R. L. Armstrong, Y. Durand, P. Etchevers, E. Greene, D. M. McClung, K. Nishimura, P. K. Satyawali, S. A. Sokratov (2009), The international classification for seasonal snow on the ground, IHP-VII Tech. Documents in Hydrol. N°83, IACS Contribution N°1, UNESCO-IHP, Paris, 90 pp.
- Flanner, M. G., C. S. Zender, J. T. Randerson, and P. J. Rasch (2007), Present day climate forcing and response from black carbon in snow, *J. Geophys. Res.*, *112*, D11202, doi:10.1029/2006JD008003.
- Flanner, M. G., C. S. Zender, P. G. Hess, N. M. Mahowald, T. H. Painter, V. Ramanathan, and P. J. Rasch (2009), Springtime warming and reduced snow cover from carbonaceous particles, *Atmos. Chem. Phys.*, *9*, 2481–2497, doi:10.5194/acp-9-2481-2009.
- Giovinetto, M. B., and W. Schwerdtfeger (1965), Analysis of a 200 year snow accumulation series from the South Pole, *Archiv für Meteorologie, Geophysik und Bioklimatologie, Serie A*, *15*(2), 227–250.
- Gleeson, D. F., R. T. Pappalardo, S. E. Grasby, M. S. Anderson, B. Beauchamp, R. Castaño, S. A. Chien, T. Doggett, L. Mandrake, and K. L. Wagstaff (2010), Characterization of a sulfur-rich Arctic spring site and field analog to Europa using hyperspectral data, *Remote Sens. Environ.*, *114*(6), 1297–1311, doi:10.1016/j.rse.2010.01.011.
- Goelles, T., C. E. Bøggild, and R. Greve (2015), Ice sheet mass loss caused by dust and black carbon accumulation, *Cryosphere*, *9*, 1845–1856.
- Grotti, M., F. Soggia, F. Ardini, and E. Magi (2011), Major and trace element partitioning between dissolved and particulate phases in Antarctic surface snow, *J. Environ. Monit.*, *13*, 2511–2520.
- Gupta, R. P. (2003), *Remote Sensing Geology*, 2nd ed., Springer, Berlin.
- Hadley, O. L., and T. W. Kirchstetter (2012), Black-carbon reduction of snow albedo, *Nat. Clim. Chang.*, *2*, 437–440.
- Hansen, A. D. A., B. A. Bodhaine, E. G. Dutton, and R. C. Schnell (1988), Aerosol black carbon measurements at the South Pole: Initial results, 1986–1987, *Geophys. Res. Lett.*, *15*, 1193–1196, doi:10.1029/GL015i011p01193.
- Hansen, J., and L. Nazarenko (2004), Soot climate forcing via snow and ice albedos, *Proc. Natl. Acad. Sci.*, *101*, 423–428.
- Hanson, K. J. (1960), Radiation measurement on the Antarctic snowfield, a preliminary report, *J. Geophys. Res.*, *65*, 935–946, doi:10.1029/JZ065i003p00935.
- Harris, J. M. (1992), An analysis of 5-day midtropospheric flow patterns for the South Pole: 1985–1989, *Tellus B*, *44*(4), 409–421.
- Hogan, A., S. Barnard, J. Samson, and W. Winters (1982), The transport of heat, water vapor and particulate material to the south polar plateau, *J. Geophys. Res.*, *87*, 4287–4292, doi:10.1029/JC087iC06p04287.
- Hoinkes, H. C. (1960), Studies of solar radiation and albedo in the Antarctic, *Archiv für Meteorologie, Geophysik und Bioklimatologie, B*, *10*(2), 175–181.
- Huheey, J. E., E. A. Keiter, R. L. Keiter (1993), *Inorganic Chemistry: Principles of Structure and Reactivity*, 4th ed., 964 pp., New York, Harper Collins.
- Hunt, G. R. (1977), Spectral signatures of particulate minerals, in the visible and near-infrared, *Geophysics*, *42*, 501–513.
- Intergovernmental Panel on Climate Change (2014), Climate change 2014: Synthesis report, Contribution of Working Groups I, II and III to the Fifth Assessment Rep. of the Intergovernmental Panel on Clim. Change, Geneva, Switz., 151 pp.
- Jacobi, H. W., S. Lim, M. Ménégoz, P. Ginot, P. Laj, P. Bonasoni, P. Stocchi, A. Marinoni, and Y. Arnaud (2015), Black carbon in snow in the upper Himalayan Khumbu Valley, Nepal: Observations and modeling of the impact on snow albedo, melting, and radiative forcing, *Cryosphere*, *9*, 1685–1699.
- Jouzel, J., L. Merlivat, J. R. Petit, and C. Lorius (1983), Climatic information over the last century deduced from a detailed isotopic record in the South Pole snow, *J. Geophys. Res.*, *88*, 2693–2703, doi:10.1029/JC088iC04p02693.
- Jung, A., J. Maier, P. Penhale, and P. Toschik (2004), *Development and Implementation of Surface Traverse Capabilities in Antarctica Comprehensive Environmental Evaluation*, p. 172, Natl. Sci. Foundation, Arlington, Va.
- Kaspari, S., T. H. Painter, M. Gysel, S. M. Skiles, and M. Schwikowski (2014), Seasonal and elevation variations of black carbon and dust in snow and ice in the Solu-Khumbu, Nepal and estimated radiative forcings, *Atmos. Chem. Phys.*, *14*, 8089–8103.
- Kaspari, S., M. Skiles, I. Delaney, D. Dixon, and T. H. Painter (2015), Accelerated glacier melt on Snow Dome, Mount Olympus, Washington, USA, due to deposition of black carbon and mineral dust from wildfire, *J. Geophys. Res. Atmos.*, *120*, 2793–2807, doi:10.1002/2014JD022676.
- Keeling, C. D., J. A. Adams Jr., C. A. Ekdahl Jr., and P. R. Guenther (1976), Atmospheric carbon dioxide variations at the South Pole, *Tellus*, *28*(6), 552–564.
- Khan, A. L., H. Dierssen, J. P. Schwarz, C. Schmitt, A. Chlus, M. Hermanson, T. H. Painter, and D. M. McKnight (2017), Impacts of coal dust from an active mine on the spectral reflectance of Arctic surface snow in Svalbard, Norway, *J. Geophys. Res. Atmos.*, *122*, 1767–1778, doi:10.1002/2016JD025757.
- Koch, D., S. Menon, A. Del Genio, R. Ruedy, I. Alienov, and G. A. Schmidt (2009), Distinguishing aerosol impacts on climate over the past century, *J. Clim.*, *22*, 2659–2677.
- Koffman, B. G., M. J. Handley, E. C. Osterberg, M. L. Wells, and K. J. Kreutz (2014), Dependence of ice-core relative trace-element concentration on acidification, *J. Glaciol.*, *60*(219), 103–112.
- Kokaly, R. F. (2011), PRISM: Processing routines in IDL for spectroscopic measurements, U.S. Geol. Surv. Open File Rep., 2011–1155, 431 pp.
- Kokaly, R. F., et al. (2017), USGS Spectral Library Version 7, *U.S. Geol. Surv. Data Ser.*, *1035*, 61 pp., doi:10.3133/ds1035.
- Korotkikh, E. V., P. A. Mayewski, D. Dixon, A. V. Kurbatov, and M. J. Handley (2014), Recent increase in Ba concentrations as recorded in a South Pole ice core, *Atmos. Environ.*, *89*, 683–687.
- Kuchiki, K., T. Aoki, T. Tanikawa, and Y. Kodama (2009), Retrieval of snow physical parameters using a ground-based spectral radiometer, *Appl. Opt.*, *48*(29), 5567–5582.
- Kuivinen, K. C., B. R. Koci, G. W. Holdsworth, and A. J. Gow (1982), South Pole ice core drilling, 1981–1982, *Antarctic J. US*, *17*(5), 89–91.
- Kumai, M. (1976), Identification of nuclei and concentrations of chemical species in snow crystals sampled at the South Pole, *J. Atmos. Sci.*, *33*, 833–841.
- LaChapelle, E. R. (1969), *Field Guide to Snow Crystals*, p. 112, Univ. of Washington Press, Seattle.
- Lazzara, M. A., L. M. Keller, T. Markle, and J. Gallagher (2012), Fifty-year Amundsen Scott South Pole Station surface climatology, *Atmos. Res.*, *118*, 240–259.

- Martonchik, J. V., C. J. Bruegge, and A. H. Strahler (2000), A review of reflectance nomenclature used in remote sensing, *Remote Sens. Rev.*, 19(1–4), 9–20.
- McClure, D. (1959), Electronic spectra of molecules and ions in crystals. Part II. Spectra of ions in 20 crystals, *Solid State Phys.*, 9, 399–525.
- McConnell, J. R., R. C. Bales, and D. R. Davis (1997), Recent intra-annual snow accumulation at South Pole: Implications for ice core interpretation, *J. Geophys. Res.*, 102, 21,947–21,954, doi:10.1029/97JD00848.
- McConnell, J. R., et al. (2014), Antarctic-wide array of high-resolution ice core records reveals pervasive lead pollution began in 1889 and persists today, *Sci. Rep.*, 4, 5848.
- McDougal, J. N., and J. V. Rogers (2004), Local and systemic toxicity of JP-8 from cutaneous exposures, *Toxicol. Lett.*, 149, 301–308.
- Miner, S. (1969), Air pollution aspects of barium and its compounds, Litton Systems, Inc., Bethesda, MD., Contract No. Ph-22-68-25, 69.
- Mosley-Thompson, E., J. F. Paskievitch, A. J. Gow, and L. G. Thompson (1999), Late 20th century increase in South Pole snow accumulation, *J. Geophys. Res.*, 104, 3877–3886, doi:10.1029/1998JD200092.
- Nazarenko, Y., U. Kurien, O. Nepotchatykh, R. B. Rangel-Alvarado, and P. A. Ariya (2016), Role of snow and cold environment in the fate and effects of nanoparticles and select organic pollutants from gasoline engine exhaust, *Environ. Sci.: Processes Impacts*, 18, 190–199.
- Negi, H. S., C. Shekhar, and S. K. Singh (2015), Snow and glacier investigations using hyperspectral data in the Himalaya, *Curr. Sci., Spec. Section: Hyperspectral Remote Sens.*, 108(5), 892–902.
- Ng, A., and C. C. Patterson (1982), Changes in lead and barium with time in California off-shore basin sediments, *Geochim. Cosmochim. Acta*, 46(11), 2307–2321.
- Nicodemus, F. E., J. C. Richmond, J. J. Hsia, I. W. Ginsberg, and T. Limperis (1977), Geometrical considerations and nomenclature for reflectance, Tech. Rep., Natl. Bureau of Standards, U.S. Dep. of Commerce, 67 pp.
- Nicolas, J. P., and D. H. Bromwich (2011), Climate of West Antarctica and Influence of Marine Air Intrusions, *J. Clim.*, 24, 49–67.
- Nolin, A. W., and J. Dozier (2000), A hyperspectral method for remotely sensing the grain size of snow, *Remote Sens. Environ.*, 74(2), 207–216.
- National Research Council (2003), *Toxicologic Assessment of Jet-Propulsion Fuel 8*, 230 pp., National Academies Press, Washington, D. C.
- O'Brien, H. W., R. H. Munis (1975), Red and near-infrared spectral reflectance of snow, CRREL Res. Rep., 332, U.S. Army Cold Regions Res. Eng. Lab., Hanover, N.H., 18 pp.
- Osterberg, E. C., M. J. Handley, S. B. Sneed, P. A. Mayewski, and K. J. Kreutz (2006), Continuous ice core melter system with discrete sampling for major ion, trace element, and stable isotope analyses, *Environ. Sci. Technol.*, 40(10), 3355–3361.
- Pacyna, J. M., and E. G. Pacyna (2001), An assessment of global and regional emissions of trace metals to the atmosphere from anthropogenic sources worldwide, *Environ. Rev.*, 9(4), 269–298, doi:10.1139/a01-012.
- Painter, T. H., and J. Dozier (2004), Measurements of the hemispherical-directional reflectance of snow at fine spectral and angular resolution, *J. Geophys. Res.*, 109, D18115, doi:10.1029/2003JD004458.
- Painter, T. H., A. P. Barrett, C. C. Landry, J. C. Neff, M. P. Cassidy, C. R. Lawrence, K. E. McBride, and G. L. Farmer (2007), Impact of disturbed desert soils on duration of mountain snow cover, *Geophys. Res. Lett.*, 34, L12502, doi:10.1029/2007GL030284.
- Painter, T. H., A. C. Bryant, and S. M. Skiles (2012), Radiative forcing by light absorbing impurities in snow from MODIS surface reflectance data, *Geophys. Res. Lett.*, 39, L17502, doi:10.1029/2012GL052457.
- Painter, T. H., F. C. Seidel, A. C. Bryant, S. M. Skiles, and K. Rittger (2013), Imaging spectroscopy of albedo and radiative forcing by light-absorbing impurities in mountain snow, *J. Geophys. Res. Atmos.*, 118, 9511–9523, doi:10.1002/jgrd.50520.
- Pirazzini, R., P. Räisänen, T. Vihma, M. Johansson, and E.-M. Tastula (2015), Measurements and modelling of snow particle size and shortwave infrared albedo over a melting Antarctic ice sheet, *Cryosphere*, 9, 2357–2381.
- Planchon, F. A. M., C. F. Boutron, C. Barbante, G. Cozzi, V. Gaspari, E. W. Wolff, C. P. Ferrari, and P. Cescon (2002), Changes in heavy metals in Antarctic snow from coastal land since the mid-19th to the late 20th century, *Earth Planet. Sci. Lett.*, 200, 207–222.
- Pluta, M. (1988), *Advanced Light Microscopy, Principles and Basic Properties*, vol. 1, p. 482, Elsevier Science, Amsterdam.
- Polashenski, C. M., J. E. Dibb, M. G. Flanner, J. Y. Chen, Z. R. Courville, A. M. Lai, J. J. Schauer, M. M. Shafer, and M. Bergin (2015), Neither dust nor black carbon causing apparent albedo decline in Greenland's dry snow zone: Implications for MODIS C5 surface reflectance, *Geophys. Res. Lett.*, 42, 9319–9327, doi:10.1002/2015GL065912.
- Qian, Y., T. J. Yasunari, S. J. Doherty, M. G. Flanner, W. K. M. Lau, M. Jing, H. Wang, M. Wang, S. G. Warren, and R. Zhang (2015), Light-absorbing particles in snow and ice: Measurement and modeling of climatic and hydrological impact, *Adv. Atmos. Sci.*, 32, 64–91.
- Radok, U., R. C. Lille (1977), A year of snow accumulation at Plateau Station, in *Meteorological Studies at Plateau Station, Antarctica, Antarctic Res. Ser.*, vol. 25, edited by J. A. Businger, pp. 17–26, AGU, Washington, D. C.
- Ricchiuzzi, P., S. R. Yang, C. Gautier, and D. Sowle (1998), SBDART: A research and teaching software tool for plane-parallel radiative transfer in the Earth's atmosphere, *Bull. Am. Meteorol. Soc.*, 79(10), 2101–2114.
- Schaepman-Strub, G., M. E. Schaepman, T. H. Painter, S. Dangel, and J. V. Martonchik (2006), Reflectance quantities in optical remote sensing—Definitions and case studies, *Remote Sens. Environ.*, 103, 27–42.
- Schroeder, H. A. (1970), *Barium, Air Quality Monograph, Air Quality Monogr. No. 70–12*, Am. Petroleum Inst., Washington, D. C.
- Schwarz, J. P., et al. (2006), Single-particle measurements of midlatitude black carbon and light-scattering aerosols from the boundary layer to the lower stratosphere, *J. Geophys. Res.*, 111, D16207, doi:10.1029/2006JD007076.
- Schwanck, F., J. C. Simões, M. Handley, P. A. Mayewski, R. T. Bernardo, and F. E. Aquino (2016), Anomalously high arsenic concentration in a West Antarctic ice core and its relationship to copper mining in Chile, *Atmos. Environ.*, 125, 257–264.
- Seidel, F., K. Rittger, S. M. Skiles, and T. H. Painter (2016), Case study of spatial and temporal variability of snow cover, grain size, albedo and radiative forcing in the Sierra Nevada and Rocky Mountain snowpack derived from imaging spectroscopy, *Cryosphere*, 10, 1229–1244, doi:10.5194/tc-10-1229-2016.
- Shirsat, S. V., and H. F. Graf (2009), An emission inventory of sulfur from anthropogenic sources in Antarctica, *Atmos. Chem. Phys.*, 9, 3397–3408.
- Simões, J. C., and V. S. Zagorodnov (2001), The record of anthropogenic pollution in snow and ice in Svalbard, Norway, *Atmos. Environ.*, 35, 403–413.
- Skiles, S. M., T. Painter, J. Deems, A. Bryant, and C. Landry (2012), Dust radiative forcing in snow of the Upper Colorado River Basin: 2. Interannual variability in radiative forcing and snowmelt rates, *Water Resour. Res.*, 48, W07522, doi:10.1029/2012WR011986.
- Skiles, S. M. (2014), Dust and black carbon radiative forcing controls on snowmelt in the Colorado River basin, PhD thesis, 274 pp., Univ. of California, Los Angeles. [Available at <http://escholarship.org/uc/item/2759r0j9>.]
- Skiles, S. M., and T. H. Painter (2016), Daily evolution in dust and black carbon content, snow grain size, and snow albedo during snowmelt, Rocky Mountains, Colorado, *J. Glaciol.*, doi:10.1017/jog.2016.125.
- Skiles, S. M., T. H. Painter, and G. S. Okin (2016), A method to retrieve the spectral complex refractive index and single scattering optical properties of dust deposited in mountain snow cover, *J. Glaciol.*, doi:10.1017/jog.2016.126.

- Stamnes, K., S.-C. Tsay, W. J. Wiscombe, and K. Jayaweera (1988), Numerically stable algorithm for discrete-ordinate-method radiative transfer in multiple scattering and emitting layered media, *Appl. Opt.*, *27*, 2502–2509.
- Stephens, M., N. Turner, and J. Sandberg (2003), Particle identification by laser-induced incandescence in a solid-state laser cavity, *Appl. Opt.*, *42*(19), 3726–3736.
- Suttie, E. D., and E. W. Wolff (1993), The local deposition of heavy metal emissions from point sources in Antarctica, *Atmos. Environ.*, *27A*(12), 1833–1841.
- Tedesco, M., C. M. Foreman, J. Anton, N. Steiner, and T. Schwartzman (2013), Comparative analysis of morphological, mineralogical and spectral properties of cryoconite in Jakobshavn Isbrae, Greenland, and Canada Glacier, Antarctica, *Ann. Glaciol.*, *54*, 63.
- Tesseraux, I. (2004), Risk factors of jet fuel combustion products, *Toxicol. Lett.*, *149*, 295–300.
- Toon, O. B., C. P. McKay, T. P. Ackerman, and K. Santhanam (1989), Rapid calculation of radiative heating rates and photodissociation rates in inhomogeneous multiple scattering atmospheres, *J. Geophys. Res.*, *94*, 16,287–16,301, doi:10.1029/JD094iD13p16287.
- Tuncel, G., N. K. Aras, and W. H. Zoller (1989), Temporal variations and sources of elements in the South Pole atmosphere 1. Nonenriched and moderately enriched elements, *J. Geophys. Res.*, *94*, 13,025–13,038, doi:10.1029/JD094iD10p13025.
- Vouk, V. B., and W. T. Piver (1983), Metallic elements in fossil fuel combustion products: Amounts and form of emissions and evaluation of carcinogenicity and mutagenicity, *Environ. Health Perspect.*, *47*, 201–225.
- Wang, X., S. J. Doherty, and J. Huang (2013), Black carbon and other light-absorbing impurities in snow across Northern China, *J. Geophys. Res. Atmos.*, *118*, 1471–1492, doi:10.1029/2012JD018291.
- Warren, S. G. (1982), Optical properties of snow, *Rev. Geophys. Space Phys.*, *20*(1), 67–89.
- Warren, S. G. (2013), Can black carbon in snow be detected by remote sensing?, *J. Geophys. Res. Atmos.*, *118*, 779–786, doi:10.1029/2012JD018476.
- Warren, S. G., and A. D. Clarke (1990), Soot in the atmosphere and snow surface of Antarctica, *J. Geophys. Res.*, *95*, 1811–1816, doi:10.1029/JD095iD02p01811.
- Warren, S. G., and W. J. Wiscombe (1980), A model for the spectral albedo of snow. II: Snow containing atmospheric aerosols, *J. Atmos. Sci.*, *37*, 2734–2745.
- Warren, S. G., C. S. Roesler, V. I. Morgan, R. E. Brandt, I. D. Goodwin, and I. Allison (1993), Green icebergs formed by freezing of organic-rich seawater to the base of Antarctic ice shelves, *J. Geophys. Res.*, *98*, 6921–6928, doi:10.1029/92JC02751.
- Warren, S. G., R. E. Brandt, and T. C. Grenfell (2006), Visible and near-ultraviolet absorption spectrum of ice from transmission of solar radiation into snow, *Appl. Opt.*, *42*(21), 5320–5334.
- Wedepohl, K. H. (1995), The composition of the continental crust, *Geochim. Cosmochim. Acta*, *59*(7), 1217–1232.
- Weingartner, E., H. Saathoff, M. Schnaiter, N. Streit, B. Bitnar, and U. Baltensperger (2003), Absorption of light by soot particles: Determination of the absorption coefficient by means of aethalometers, *J. Aerosol Sci.*, *34*, 1445–1463.
- Wendl, I. A., J. A. Menking, R. Fäber, M. Gysel, S. Kaspari, M. Laborde, and M. Schwikowski (2014), Optimized method for black carbon analysis in ice and snow using the single particle soot photometer, *Atmos. Meas. Tech.*, *7*, 2667–2681.
- Wientjes, I. G. M., and J. Oerlemans (2010), An explanation for the dark region in the western melt zone of the Greenland ice sheet, *Cryosphere*, *4*, 261–268, doi:10.5194/tc-4-261-2010.
- Wiscombe, W. J., and S. G. Warren (1980), A model for the spectral albedo of snow. I. Pure snow, *J. Atmos. Sci.*, *37*, 2712–2733.
- Zege, E., I. Katsev, A. Malinka, A. Prikhach, and I. Polonsky (2008), New algorithm to retrieve the effective snow grain size and pollution amount from satellite data, *Ann. Glaciol.*, *49*, 139–144.
- Zege, E. P., I. L. Katsev, A. V. Malinka, A. S. Prikhach, G. Heygster, and H. Wiebe (2011), Algorithm for retrieval of the effective snow grain size and pollution amount from satellite measurements, *Remote Sens. Environ.*, *115*, 2674–2685.